Hysterons and pathways in mechanical metamaterials

Ding, J.

CHAPTER 2

EMBEDDING A MECHANICAL HYSTERON IN A BIHOLEY METAMATERIAL

2.1 Motivation

Driven frustrated mechanical systems have shown complex intermittent behavior, featuring reversibly smooth deformations in meta-stable states and sharp transitions between these states [1–3, 5, 16, 33, 40–43]. In mechanical systems, these irreversible and hysteric transitions are often associated with the snapping of local elements called hysterons [17, 18, 44–48]. When the external driving strain passes the critical (un)snapping strain of a hysteron, its state is modified. These hysterons can be thought of as mechanical bits that can be in two states that we call 0 and 1 [17, 18, 44, 50, 51]. In this chapter, we introduce a strategy to embed hysterons in a metamaterial.

Our strategy to obtain controlled hysterons is creating frustration [1–3, 5, 6, 52, 53]. For instance, introducing a defect [2, 3, 5, 6, 12, 41, 54, 55] in a periodic structure may lead to frustration. External driving of a material with such a defect may cause competition between the local deformation and global deformation, and eventually causes bistability.

Here we create bistable defects in a 2D biholey metamaterial. We note that the deformations of a holey sheet, compressed in y-direction, causes the bigger holes to become x-polarized ellipses [2, 3, 11, 30, 34–39] (Fig. 2.1). The hourglass part between two holes, as shown in Fig. 2.1a, is an atypical beam that bends to the right under compression. However, a beam initially curving to the left will bend more to the left under compression. Here we replace one hourglass-shaped part, which bends to the right in biholey structure, with a defect beam initially curving to the left. The deformation of this defect beam will be set by a competition between left and right bending. We anticipate that when the sample is compressed, such defect beam will either bend to the right, bend to the left, or show bistable states including both bending and snapping.

In this chapter, we study all possible actions of such a defect beam in a biholey metamaterial by varying its geometry. We first discuss the geometry of the metamaterial with a defect beam in Section 2.2. Next, we discuss the possible behaviors that we observe when varying the parameters of the defect beam (Section 2.3). Then we discuss the appropriate design for snapping action and how to tune the snapping and unsnapping strains (Section 2.5). Finally, we discus the boundary conditions of the defect (Section 2.4). Throughout this chapter, we focus on numerical simulations.

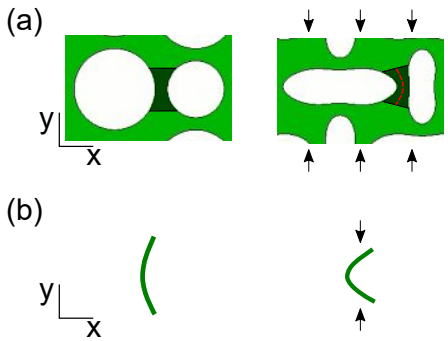

FIGURE 2.1: Uncompressed and compressed structures, where the black arrows denote the compression direction. (a) Detail of an biholey metamaterial under compression. An hourglass shaped part between two holes is highlighted by gray. We observe that the center of the hourglass shaped part (red dash line) bends to the right under compression. (b) Schematic of a pre-curved beam under compression. We observe that the beam bends to the left under compression.

2.2 Geometry and approach

2.2.1 Geometry

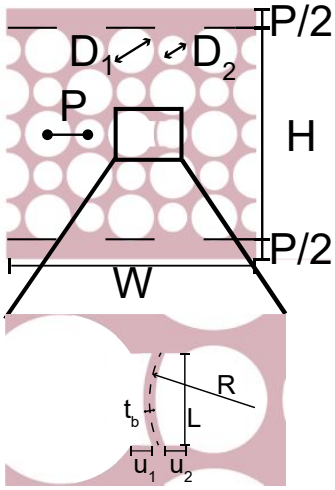

FIGURE 2.2: Geometry of a quasi-2D biholey metamaterial with a defect beam, which is characterized by its length L, radius of curvature R, thickness t_b, and location (u_1, u_2). Zoom-in: geometry of the defect beam.

To create frustration, we embed a defect in the biholey metamaterial, as shown in Fig. 2.2. The biholar metamaterial with a defect beam features a square array of alternating circular holes of diameter D_1 and D_2. We focus here on biholey metamaterials consisting of 5×5 holes. To ensure homogenous loading, we extend the top and bottom parts by $P/2$; the effective height of the sample, H, is defined as $m \times P$, where P is the pitch of the array and $m = 5$ is the number of holes in the vertical direction. The defect beam is specified by the length L, its dimensionless radius of curvature $r := R/L$, dimensionless thickness $t := t_b/L$, and dimensionless horizontal location $u := \frac{u_1 - u_2}{u_1 + u_2}$, where the defect beam is closer to the smaller (larger) holes when $u > 0$ ($u < 0$), as shown in Fig. 2.2. Based on preliminary simulation results, we fix the holey array parameters as

$\{P, D_1, D_2\} = \{10\text{mm}, 10\text{mm}, 7\text{mm}\}$, and vary the beam length L, dimensionless beam radius r, dimensionless beam offset u and dimensionless beam radius t, and determine the behavior of the resulting defect beams.

2.2.2 Numerical method

We used Abaqus FEM simulations to investigate the behavior of an individual defect beam. We use a 2D structure, and model the rubber metamaterial with neo-Hookean hyper elastic model, using 4-node bilinear plane strain quadrilaterals, reduced integration and hourglass control (CPD4R). We have performed a systematic mesh refinement study for the in-plane grid, leading to an optimal mesh size of $t/3$. The parameters of our incompressible isotopic neo-Hookean material, C_{10} and D_1, are given by the shear modulus and bulk modulus, μ and K, which are described by the Poisson's ratio of the rubber (ν = 0.495) and the Young's modulus (E = 220 KPa).

$$\begin{aligned} C_{10} &= \tfrac{1}{2}\mu \\ D_1 &= \tfrac{2}{K} \\ \mu &= \tfrac{E}{2(1+\nu)} \\ K &= \tfrac{E}{3(1-2\nu)} \end{aligned} \tag{2.1}$$

To dissipate the kinetic energy caused by snapping, we apply damping to model, and the critical damping factor is:

$$C = \frac{\alpha_R}{2\omega_i} + \frac{\beta_R \omega_i}{2} \tag{2.2}$$

where ω_i is the natural frequency; α_R = 0.1; β_R = 0.

To observe the action of the defect beam, we apply compression on the top surface of the sample and fix the bottom surface, track the center part of the defect beam which is defined as U_x, thus obtaining traces $U_x(\varepsilon)$. We detect the snapping and unsnapping strain by finding peaks in $U_x(\varepsilon)$, which we do by requiring that its (numerical) derivative exceeds ten times its mean value.

2.3 Actions of the beam controlled by geometry

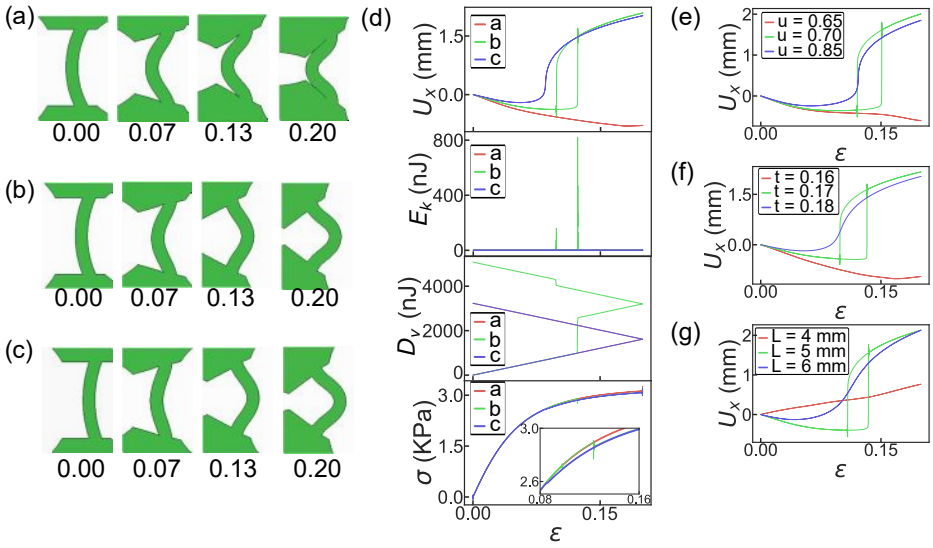

FIGURE 2.3: Behavior of the defect beam in a biholey sample, where the biholey array has $\{P, D_1, D_2\} = \{10\text{mm}, 10\text{mm}, 7\text{mm}\}$ [1]. (a - c) Under compression, the defect beam (a) co-bends (r = 1.1), (b) snaps (r = 1.3), or (c) counter bends (r = 1.5) depending on the geometry. All defect beams shown in (a - c) have $\{L, t, u\}$ = {5 mm, 0.16, 0.5 }. (d) U_x, E_k (kinetic energy), D_v (Viscous dissipation) and σ (stress), as functions of ε of the beams shown in (a), (b) and (c). Note that for the beam shown in (b) we observe hysteresis. (e) U_x as a function of u and ε, where the samples are characterized with $\{L, r, t\}$ = {5 mm, 1.1, 0.16 }. (f) U_x as a function of t and ε, where the samples are characterized with $\{L, r, u\}$ = {5 mm, 1.3, 0.25 }. (g) U_x as a function of L and ε, where the samples are characterized with $\{r, u, t\}$ = {1.2, 0.35, 0.17 }.

To explore the possible actions of the defect beams under compression, we simulate the cyclic compression process on a 5×5 sample with a defect beam. We vary one parameter of the beam and fix the rest parameters to get a range of behaviors, including counter bending, snapping, and co-bending. In the following, we study the dimensionless radius, r, the dimensionless offset, u, the dimensionless thickness, t, and the length, L.

[1] This work was carried out in collaboration with Jingran Liu.

First, we fix $\{L, t, u\} = \{5\text{mm}, 0.16, 0.5\}$ and vary r. Fig. 2.3a shows the co-bending behavior of the defect beam in the loading process, where the curvature keeps the same direction as its initial direction. We see the beam bends further to the left as the strain $\varepsilon := E_y/H$ increases, where E_y denotes the displacement of the compression plate. The displacement of the middle point of the defect beam, U_x, is shown by the red curve in Fig. 2.3d. At the same time, the curves of both the compression and decompression processes coincide. This means that in the decompression process, the beam unbends in the same way as it bends: there is no hysteresis.

Fig. 2.3b shows snapshots of a beam snapping in the loading process. In the early stage of compression process ($\varepsilon < 0.12$), the beams firstly bends to the left. Then it suddenly snaps to the right at $\varepsilon = 0.12$ because of the rotation of its boundaries. We refer to the snapping strain as ε^+, and ε_i^- for unsnapping. After snapping, the beam bends to the right. In the early stage of the decompression process ($\varepsilon > 0.10$), the beam unbends smoothly. Then the beam snaps back at $\varepsilon^- = 0.10$, where ε^- denotes the unsnapping strain. The (un)snapping behavior of the defect beam releases kinetic energy, E_k, which eventually dissipates due to the viscoelasticity, D_v, of the rubber. As a result, we observe a sharp peak in $E_k - \varepsilon$ curve and a sharp jump in the $D_v - \varepsilon$ curve when the beam (un)snaps. At the same time, we observe that the (un)snapping behavior is visible as a small jump in the compressive stress $\sigma := F/(WT)$, where F is the compressive force. We note that the beam acts hysterically in this case.

We observe that U_x drastically changes when the defect beam (un)snaps, and there are obvious differences between snapped and unsnapped configuration of the defect beam — the unsnapped beam curves to the left while the snapped beam curves to the right. We note that $\varepsilon^- < \varepsilon^+$, so there is a bistable region in $\varepsilon^- < \varepsilon < \varepsilon^+$ where the defect beam can bend to the left or to the right. Therefore, we can model the defect beam in a compressed sample as a hysteron. The unsnapped state can be considered as state '0' and snapped state can be considered as state '1'. The defect beam flips it from '0' to '1' at ε^+ and flips from '1' to '0' at ε^-.

Fig. 2.3c shows snapshots of the counter bending behavior of the defect beam in the loading process. When the holes in the biholey metamaterial start to form an orthogonal ellipse pattern, the beam slowly bends in the opposite direction from its initial direction. In the decompression process, the trace of the beam going back in the decompression process coincides with its trace in the compression, as shown by the blue curve in Fig. 2.3d. Hence, the beam motion is smooth and there is no hysteresis.

We are able to get a range of behaviors of the defect beam by modifying its parameters, r, u, t, and L. Firstly, we sequentially observe the co-bending, snapping, and counter bending behavior of the defect beam as u increases (Fig. 2.3e). We interpret this as follows: due to the rotation of the diamonds, the effective distance between the top and bottom of the defect increase as u increases so that the beam with larger u is less compressed (Section 2.4). Next, we sequentially observe the co-bending, snapping, and counter bending behavior of the defect beam as t increases (Fig. 2.3f) — slender beams are easier to co-bend than a thicker beam in the same boundaries condition. Finally, we sequentially observe the co-bending, snapping, and counter bending of the defect beam as L increases (Fig. 2.3g). Hence, the snapping behavior of the beams can be controlled by all geometric parameters.

In conclusion, we can control the opposite effects of the buckling of a defect beam and the (rotational) deformations of its endpoints by the geometric design of the defect beam. With a range of parameters, we observe different behaviors of the defect under quasi-static compression, including co-bending, snapping and counter bending. For cyclical compression, the (un)snapping behavior exhibits hysteresis, and ε^+ is larger than ε^-.

2.4 Interpretation: boundary conditions of the defect beam

To understand the various deformation modes of the defect beam, we now consider the deformations of a biholey metamaterial, without defect beams, in detail. We assume that as the defect beam is slender, its boundary conditions, given by the translational and rotational 'islands' above and below it, can be determined from their motion in a system without defects. We investigate the evolution of a unit cell of a biholey sheet by Finite Element Method (FEM) simulations (Fig. 2.4 (a-b)), and characterize the deformation by the displacements L of the islands above and below a single beam.

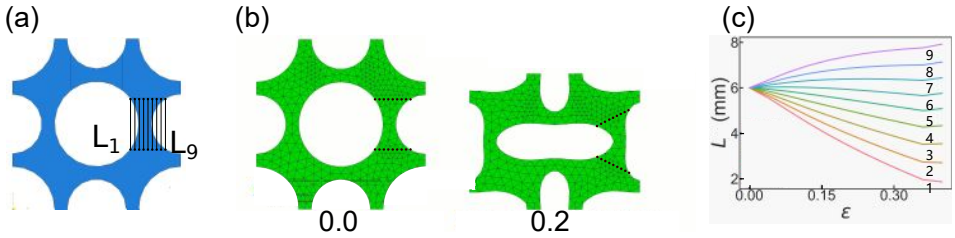

FIGURE 2.4: FEM simulations of a unit cell of biholey metamaterial under vertical compression. The unit cell has $\{P, D_1, D_2\}$ = {10 mm, 10 mm, 7 mm}. (a) The sketch of the unit cell for a range of compressions. From left to right, the distance between the top boundary and bottom boundary of the hourglass part are denoted as $L_1, L_2, L_3 ... L_9$. (b) Evolution of the unit cell. (c) $L_1, L_2, L_3 ... L_9$ as functions of ε. For details, see text.

We characterize the rotation and translational of the boundaries of the defect beam by FEM simulations on a unit cell of the biholey metamaterial under vertical compression. To investigate the boundary conditions of the defect beam, we track a series of points. As shown in Fig. 2.4a, we study a virtual beam with L = 6 mm and -1 < u < 1 and track a range of points that were symmetrical up and down and 3 mm perpendicular to the center of the hourglass part. The points we tracked on the unit cell form the effective boundary for defect beams, and are shown by nine pairs of black dots in Fig. 2.4 (a - b). Fig. 2.4 (b) shows the evolution of the unit cell under compression. To study the rotation and compression of the islands,

we track the vertical distances, L_i ($1 \leq i \leq 9$), between the nine pairs of black dots, as shown by the black vertical lines in Fig. 2.4 (a). From left to right, we label the black vertical lines in Fig. 2.4 (a) as $L_1, L_2, L_3 ... L_9$, and the evolution of L_1 to L_9 is shown in Fig. 2.4 (c).

We first notice that the upper and lower boundaries of the hourglass part are counter-rotated, this rotation is the main cause of the beam curing to the right. Secondly, in Fig. 2.4c we observe that the values of L_1 to L_9 are different — the left side of the hourglass part is compressed more than the right side. We suggest the boundaries of the defect beam are counter-rotated and move vertically when the sample is compressed. As a result, the defect beams are able to show different behaviors under such boundary conditions, and proper design is needed for snapping events.

2.5 Appropriate design for snapping

u \ r	1.1	1.15	1.2	1.3	1.4	1.5
0.25	-	-	left	left	left	bend
0.40	-	-	-	left	left	-
0.45	-	-	-	left	snap	-
0.50	left	-	left	snap	snap	right
0.55	left	left	left	snap	-	-
0.60	left	left	snap	snap	-	-
0.65	left	snap	snap	snap	-	
0.70	snap	snap	snap	-	-	-
0.75	snap	snap	right	right	right	-
0.80	snap	right	-	-	-	-
0.85	right	-	-	-	-	
1.00	-	-	right	right	right	right

TABLE 2.1: Actions of the defect beam in a biholey sample under compression, where 'left' denotes co-bending, 'snap' denotes hysteretic snapping, and 'right' denotes counter bending. The biholey array has $\{P, D_1, D_2\} = \{10\text{mm}, 10\text{mm}, 7\text{mm}\}$ and the defect beams have $\{L, t\}$ = {5 mm, 0.16}. $\varepsilon^{\pm}$ of the snapping beam is shown in Fig. 2.5.

u \ r	1.1	1.2	1.3	1.4	1.5
0.00	-	-	-	-	left
0.10	-	-	-	-	snap
0.15	-	-	-	left	snap
0.20	-	-	left	snap	snap
0.25	-	left	snap	snap	right
0.30	left	snap	snap	snap	-
0.35	left	snap	snap	right	-
0.40	left	snap	right	-	-
0.45	left	snap	-	-	-
0.50	snap	snap	-	-	right
0.55	snap	right	-	-	-
0.60	right	-	-	-	-

TABLE 2.2: Actions of the defect beam in a biholey sample under compression, where 'left' denotes co-bending, 'snap' denotes hysteretic snapping, and 'right' denotes counter bending. The biholey array has $\{P, D_1, D_2\} = \{10\text{mm}, 10\text{mm}, 7\text{mm}\}$ and the defect beams have $\{L, t\}$ = {5 mm, 0.17}. $\varepsilon^{\pm}$ of the snapping beam is shown in Fig. 2.5.

In Fig. 2.3, we observe that not all the parameters lead to (un)snapping behavior. To obtain snapping events, we should use appropriate values of the parameters. Here we explore the parameter space suitable to find snapping and control the critical strains $\varepsilon^{\pm}$.

Table 2.1 and Table 2.2 shows the behavior of the defect beam with various values of r and u. We observe that there is a limited range of parameters that lead to snapping. For example, when $r = 1.1$, $u = 0.70$ to 0.80, the beam snaps but when r = 1.1 and u = 0.10 to 0.20, the beam co-bends. Based on the data in Table 2.1 and Table 2.2, we believe that intermediate values are needed for snapping.

Fig. 2.5 shows $\varepsilon^{\pm}$ as a function of r, t and u. We observe that the ε^{+} co-bends as u increases, while ε^{-} increases with u. As a function of radius r, we observe that $\varepsilon^{\pm}$ increases with r, and ε^{+} increases faster than ε^{-}. For a beam with larger r, more compression is needed to induce snapping and less

decompression is able to promote unsnapping. We note that ε^+ is always larger than ε^-, even if ε^+ and ε^- are close.

In conclusion, to observe hysteresis, the geometry of the defect beam should have appropriate values — within this range, we can tune $\varepsilon^{\pm}$.

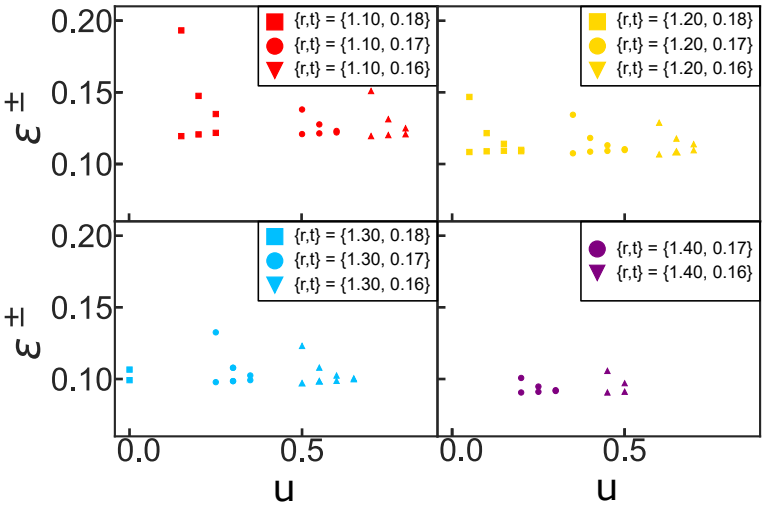

FIGURE 2.5: $\varepsilon^{\pm}$ as a function of r, t and u, where $L = 5$ mm [2]. There is hysteresis for each sample: the upper dot denotes ε^+ and the lower dot denotes ε^-. The dots almost overlapping denotes small hysteresis.

2.6 Conclusion

In this chapter, we have introduced a strategy to create mechanical hysterons being placing a defect beam into a biholey metamaterial. We obtain different behaviors of the defect beam by varying the geometry, including co-bending, snapping, and counter bending events. In particular, we show that there is hysteresis in the snapping action for appropriate designs. We

[2] This work was carried out in collaboration with Jingran Liu.

find that the (un)snapping strain can be tuned by the geometry of the defect beam.